

Experimental Investigation of an Eight Qubit Unit Cell in a Superconducting Optimization Processor

Part II: Unit Cell Performance

Richard Harris, Mohammad Amin, Neil Dickson, Mark Johnson,
Kamram Karimi, Trevor Lanting, Colin Truncik

D-Wave Systems Inc.
Burnaby, BC Canada

September 2010

Primary Reference: Harris *et al.*, Phys. Rev. B **82** 024511 (2010).

Outline

- 1 Brief Recap
- 2 Qubit and Coupler Characterization
- 3 Performance of a Unit Cell
- 4 Dynamical Model of a Unit Cell
- 5 Open Questions and What Lies Ahead
- 6 Conclusions

Outline

- 1 Brief Recap
- 2 Qubit and Coupler Characterization
- 3 Performance of a Unit Cell
- 4 Dynamical Model of a Unit Cell
- 5 Open Questions and What Lies Ahead
- 6 Conclusions

Adiabatic Quantum Optimization (AQO)

Let there be an optimization problem of the form

$$E(\vec{s}) = - \sum_i h_i s_i + \sum_{i,j>i} K_{ij} s_i s_j \quad (1)$$

where $-1 \leq h_i, K_{ij} \leq +1$ and $s_i = \pm 1$. There exists an optimal solution \vec{s}_{gs} that minimizes the objective E . Map problem onto a quantum Ising spin glass (QSG) Hamiltonian

$$\frac{\mathcal{H}_{\text{QSG}}(t)}{E_0(t)} = - \sum_i h_i \sigma_z^{(i)} + \sum_{i,j>i} K_{ij} \sigma_z^{(i)} \sigma_z^{(j)} - \Gamma(t) \sum_i \sigma_x^{(i)}. \quad (2)$$

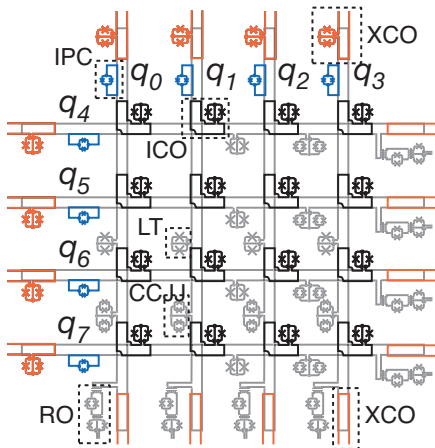
Use physical system to find the $|\vec{s}_{gs}\rangle$ by evolving $\Gamma(t)$ such that

$$\begin{aligned} \Gamma(0) &\gg h_i, K_{ij} \\ \Gamma(t_f) &\ll h_i, K_{ij} \end{aligned}$$

where t_f is the run time of the algorithm.

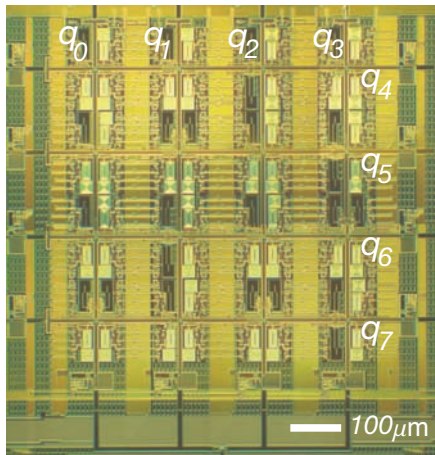
A Network of Inductively Coupled Flux Qubits

Use flux qubits as quantum Ising spins. Provide tunable mutual inductances between qubits to implement pairwise interactions.



Fabricated Device

An eight-qubit unit cell in a scalable device architecture.



Can one solve Ising spin glass problems with this unit cell?

Outline

- 1 Brief Recap
- 2 Qubit and Coupler Characterization**
- 3 Performance of a Unit Cell
- 4 Dynamical Model of a Unit Cell
- 5 Open Questions and What Lies Ahead
- 6 Conclusions

Flux Qubit Characterization

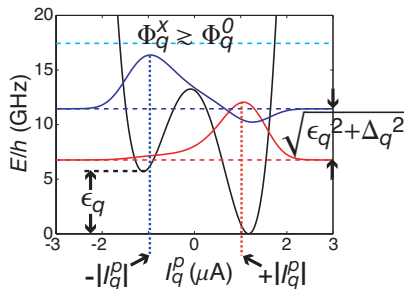
We first need to confirm that we have the requisite behavior of the qubits. The physics of the two lowest levels of a flux qubit are captured by

$$\mathcal{H}_q = -\frac{1}{2} [\epsilon_q \sigma_z + \Delta_q \sigma_x]. \quad (3)$$

$$\epsilon_q = 2 |I_q^p| (\Phi_q^x - \Phi_q^0)$$

$$|I_q^p| \equiv \text{qubit persistent current}$$

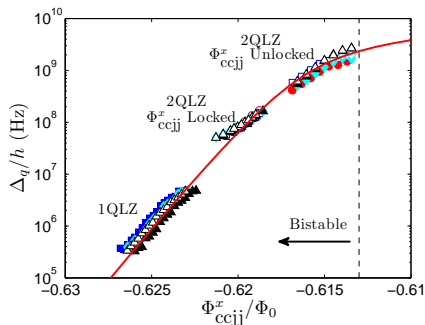
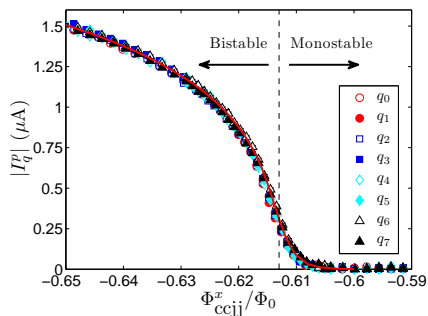
$$\Delta_q \equiv \text{qubit tunneling energy}$$



$|I_q^p|$ can be measured using readouts and other qubits as sensors. Δ_q can be quantified by using Landau-Zener experiments.

Qubit Calibration

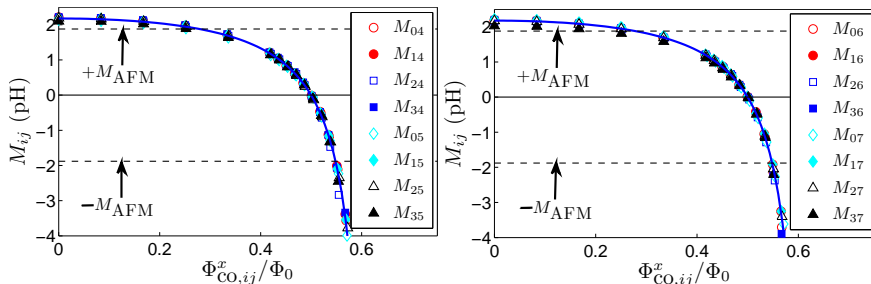
Flux qubit parameters, $|I_q^p|$ and Δ_q , versus annealing bias Φ_{ccjj}^x .



Solid curves are *predictions* of independently calibrated CCJJ rf SQUID Hamiltonian. The experimental results agree with an independent calculation of the defining properties of a flux qubit.

Coupler Calibration

Calibration of all 16 internal couplers in a unit cell. Solid curves are the same theoretical curve in both plots.



We have slightly reduced M_{AFM} on account of a coupler located in a different unit cell on the same chip.

Outline

- 1 Brief Recap
- 2 Qubit and Coupler Characterization
- 3 Performance of a Unit Cell**
- 4 Dynamical Model of a Unit Cell
- 5 Open Questions and What Lies Ahead
- 6 Conclusions

Optimization Problem Test Set

The hardware is designed to solve Ising spin glass (ISG) optimization problems of the form

$$E(\vec{s}) = - \sum_i h_i s_i + \sum_{i,j>i} K_{ij} s_i s_j$$

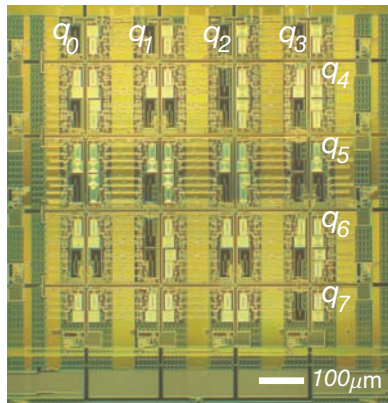
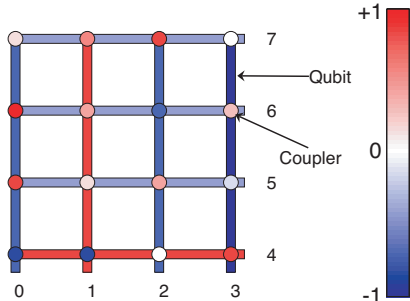
where $-1 \leq h_i, K_{ij} \leq +1$ and $s_i = \pm 1$. There exists an optimal solution \vec{s}_{gs} that minimizes E . A set of 6400 ISG problem instances that fit on a unit cell were generated by randomly drawing h_i and K_{ij} from the following set:

$$h_i, K_{ij} \in [-1 \quad -6/7 \quad -5/7 \quad \dots \quad +5/7 \quad +6/7 \quad +1].$$

We denote such a problem as being specified to 4 bits of precision (4BOP), where h_i, K_{ij} are sampled from $2^4 - 1$ evenly spaced values between ± 1 .

Embedding Problem Instances into the Hardware

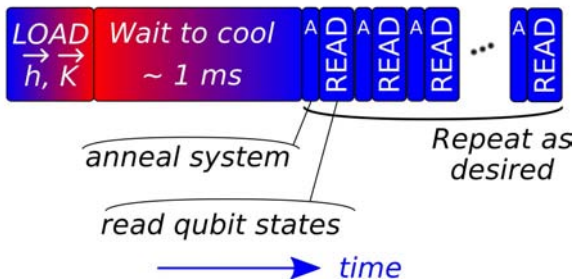
Each problem instance required 8 values of h_i and 16 values of K_{ij} to be embedded in the $|I_q^P|$ compensators and interqubit couplers, respectively.



Running Problem Instances on the Hardware

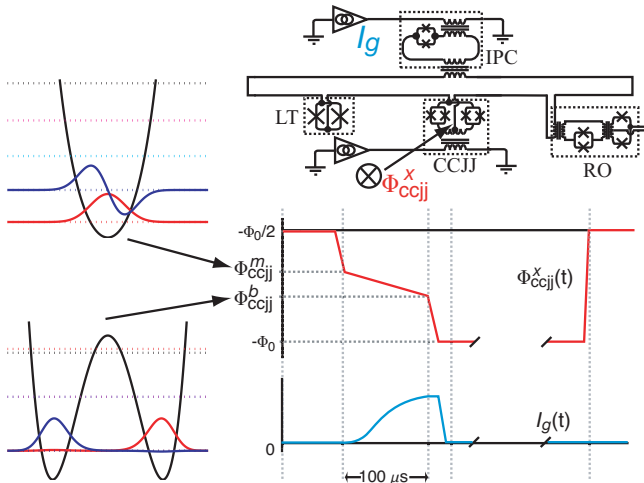
Programming of h_i and K_{ij} requires using the PMM demultiplexing circuit which dissipates energy. A 1 ms wait is inserted to allow the chip to cool back to the mixing chamber temperature. Annealing and readout are run repeatedly thereafter.

Chip Level Timing Diagram



Annealing Waveforms

During annealing there were only two time-dependent analog biases supplied to the entire unit cell - all static biases were provided by PMM.

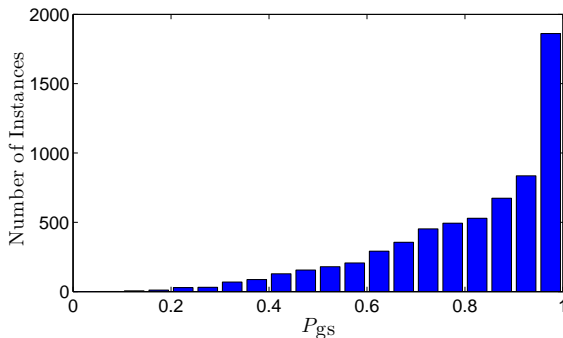


Characterizing Performance

- Run all 6400 problem instances 1000 times each and record the number of times each of the possible $2^8 = 256$ final spin configurations was observed.
- Since the problem instances were small, we could easily independently determine the ground state $|\vec{s}_{\text{gs}}\rangle$. Let the probability of observing the ground state be denoted as P_{gs} .
- All 6400 problem instances were run at three processor temperatures: 20, 35 and 50 mK. Histograms of P_{gs} were generated.

Success Histogram at $T = 20$ mK

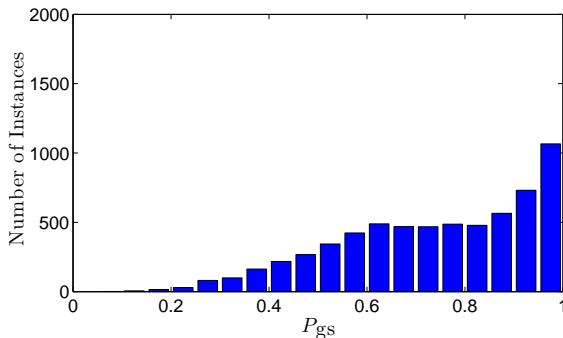
Run all 6400 problem instances at $T = 20$ mK. Take the resultant set of 6400 values of P_{gs} and generate a histogram.



Considerable probability within $0.95 < P_{gs} \leq 1$. However, there is a tail that extends to lower probability. $P_{gs} > 0.1$ for all problem instances.

Success Histogram at $T = 35$ mK

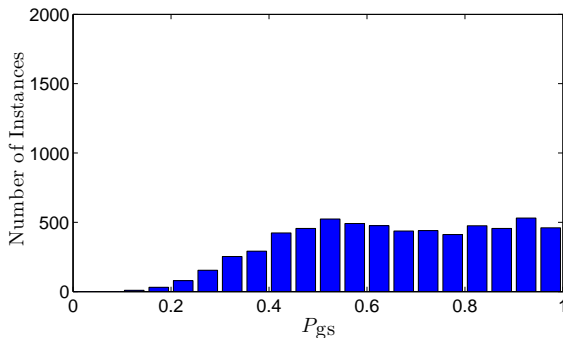
Run all 6400 problem instances at $T = 35$ mK. Take the resultant set of 6400 values of P_{gs} and generate a histogram.



Peak at $0.95 < P_{gs} \leq 1$ diminished. Broad hump centered about $P_{gs} \sim 0.6$ was observed. $P_{gs} > 0.1$ for all problem instances.

Success Histogram at $T = 50$ mK

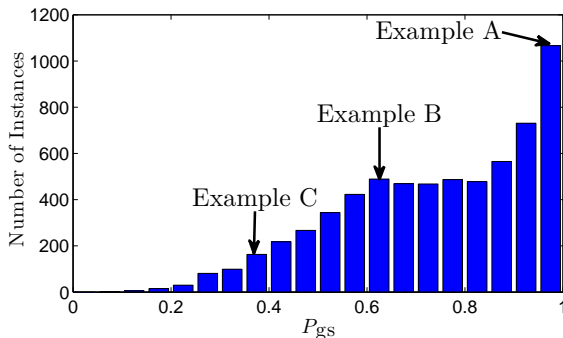
Run all 6400 problem instances at $T = 50$ mK. Take the resultant set of 6400 values of P_{gs} and generate a histogram.



Peak at $0.95 < P_{gs} \leq 1$ absent. Broad hump has shifted downward to $P_{gs} \sim 0.5$. $P_{gs} > 0.1$ for all problem instances.

Example Instances Selected from $T = 35$ mK Results

Why is there structure in the P_{gs} histograms?



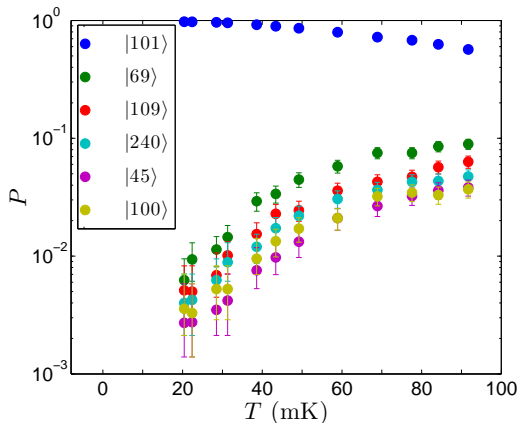
Select Example instances A, B, and C from the spike, hump and tail, respectively. Run these examples at multiple temperatures and examine probabilities P of all possible final spin configurations $|\vec{s}\rangle$.

Some Notation

Spin notation of the form $|\vec{s}\rangle = |s_0 \ s_1 \ \dots \ s_7\rangle$, with $s_i = \pm 1$, is clumsy. Use a more compact notation in which binary words $|\vec{s}\rangle$ are converted into decimal numbers $|\text{State}\rangle$:

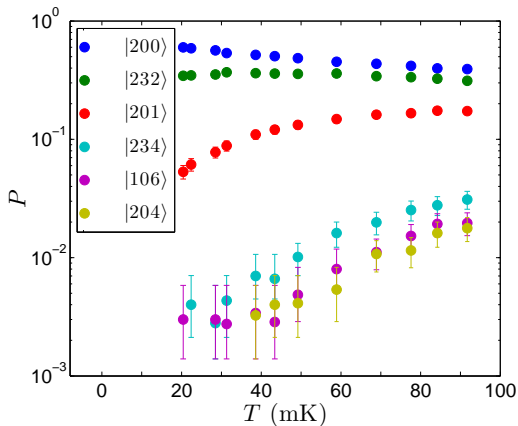
$ \vec{s}\rangle$	$ \text{Number}\rangle$
$ -1 \ -1 \ -1 \ -1 \ -1 \ -1 \ -1 \ -1 \rangle$	$ 0\rangle$
$ -1 \ -1 \ -1 \ -1 \ -1 \ -1 \ -1 \ +1 \rangle$	$ 1\rangle$
$ -1 \ -1 \ -1 \ -1 \ -1 \ -1 \ +1 \ -1 \rangle$	$ 2\rangle$
.	.
.	.
.	.
$ +1 \ +1 \ +1 \ +1 \ +1 \ +1 \ +1 \ +1 \rangle$	$ 255\rangle$

Example A Probabilities versus Temperature



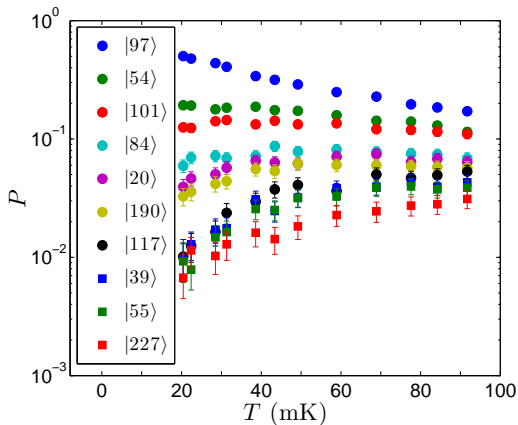
Relatively few states were observed. Probabilities of all but the ground state $|101\rangle$ increase with T .

Example B Probabilities versus Temperature



Relatively few states were observed. Probabilities of all but the ground state $|200\rangle$ and state $|232\rangle$ increase with T .

Example C Probabilities versus Temperature



More states were observed as compared to Examples A and B. Appears that probabilities of all states are converging with increasing T .

Summary of Experimental Results

Key observations from the experiments:

- 6400 randomly generated Ising spin glass problem instances were posed to an 8-qubit unit cell. The hardware returned the expected ground state as the most probable state in all instances.
- Temperature-dependent structure in the success histograms was observed.
- Three example problem instances were studied in detail as a function of temperature. The results demonstrated that only a small number of final spin configurations were observed with appreciable probability.

Can we make sense of these results? We need a quantitative model ...

Outline

- 1 Brief Recap
- 2 Qubit and Coupler Characterization
- 3 Performance of a Unit Cell
- 4 Dynamical Model of a Unit Cell**
- 5 Open Questions and What Lies Ahead
- 6 Conclusions

Closed System Hamiltonian

Given the h_i and K_{ij} for any problem instance and device parameters, the Hamiltonian describing the hardware at time t is given by

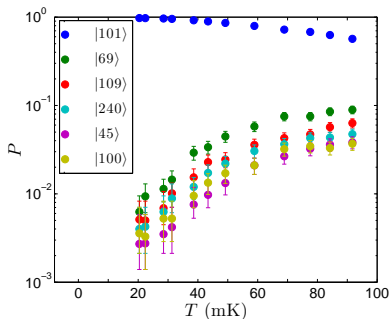
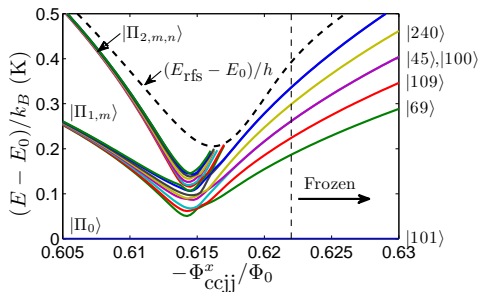
$$\frac{\mathcal{H}_0(t)}{E_0(t)} = - \sum_i h_i \sigma_z^{(i)} + \sum_{i,j>i} K_{ij} \sigma_z^{(i)} \sigma_z^{(j)} - \Gamma(t) \sum_i \sigma_x^{(i)} \quad (4a)$$

$$E_0(t) = M_{\text{AFM}} |I_q^p(t)|^2 \quad (4b)$$

$$\Gamma(t) = \frac{\Delta_q(t)}{2E_0(t)} \quad (4c)$$

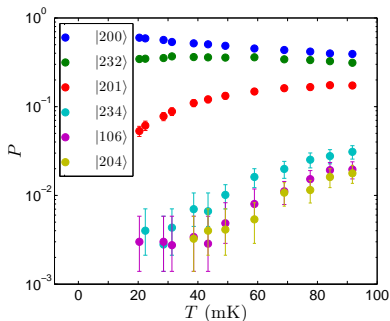
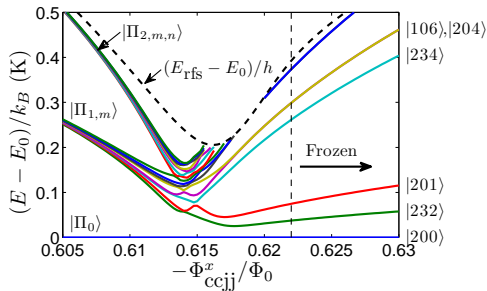
All device parameters have been independently calibrated. As a first step, one can generate eigenspectra versus annealing parameter $\Phi_{\text{ccjj}}^x(t)$ for the example problem instances A, B, and C to garner insight.

Example A Eigenspectrum versus Annealing Parameter



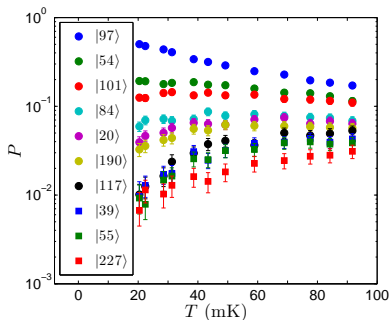
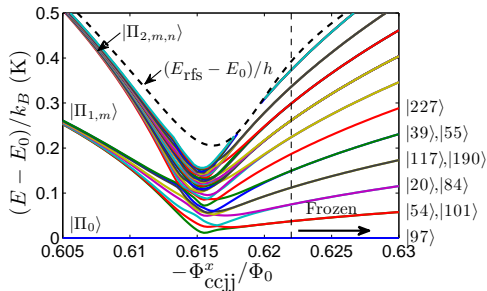
- Excited states well separated from ground state.
- Order of states in ascending E matches that in descending P .
- Population statistics 'roughly' match Boltzmann distribution at $\Phi_{ccjj}^x/\Phi_0 \approx -0.621$.

Example B Eigenspectrum versus Annealing Parameter



- Two excited states within $O(k_B T)$ of ground state.
- Again, order of states in ascending E matches that in descending P .
- Population statistics 'roughly' match Boltzmann distribution at $\Phi_{ccjj}^x/\Phi_0 \approx -0.621$.

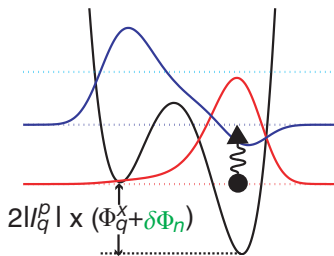
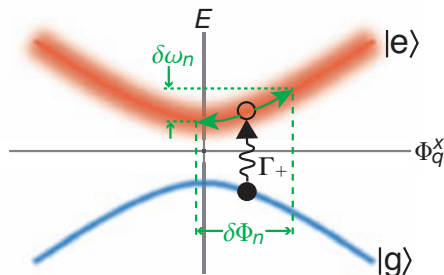
Example C Eigenspectrum versus Annealing Parameter



- Many degenerate excited states within $O(k_B T)$ of ground state.
- Again, order of states in ascending E matches that in descending P .
- Population statistics 'roughly' match Boltzmann distribution at $\Phi_{ccjj}^x / \Phi_0 \approx -0.621$.
- However, slight disparity in P for degenerate pairs ($|54\rangle, |101\rangle$) and ($|117\rangle, |190\rangle$).

Thermalization of Flux Qubits

Thermalization requires coupling of qubits to an environment (noise). Flux noise (σ_z) is the predominant concern for flux qubits.



Noise Type

'Atomic' Mode

'Ising' Mode (QA)

" T_1 "

Excitation/Relaxation

Loss of P_{gs} , Spectral Broadening

" T_ϕ "

Dephasing $\propto \delta\omega_n$

Flux Noise $\delta\Phi_n$, Loss of Precision

Open System Hamiltonian

Each qubit i is coupled to flux noise via an environmental operator $\Phi_n^{(i)}$:

$$\mathcal{H}(t) = \mathcal{H}_0(t) + \frac{1}{2} \sum_{i=0}^7 2 |I_q^p(t)| \Phi_n^{(i)}(t) \sigma_z^{(i)}. \quad (5)$$

Assuming an Ohmic noise spectral density,

$$\begin{aligned} S_i(\omega) &\equiv (2 |I_q^p(t)|)^2 \int dt' e^{i\omega t'} \langle \Phi_n^{(i)}(t') \Phi_n^{(i)}(0) \rangle \\ &= 2 \text{Im} \{L_0\} (2 |I_q^p(t)|)^2 \frac{\hbar\omega}{1 - \exp\left(-\frac{\hbar\omega}{k_B T}\right)}, \end{aligned} \quad (6)$$

$\text{Im} \{L_0\}$ is the *only* new parameter in the model - everything else has been independently calibrated. We have estimated $L_0 \approx 47$ yH·s from the width of a resonant tunneling process [see Harris *et al.*, Phys. Rev. B **82** 024511 (2010).].

Numerical Simulations

The dynamical model involves solving a series of coupled first order differential equations for the eight-qubit system's density matrix ρ :

$$\partial_t \rho_{mn} = -i\omega_{mn}\rho_{mn} - \sum_{k,l} (R_{mnkl} + M_{mnkl}) \rho_{kl}, \quad (7a)$$

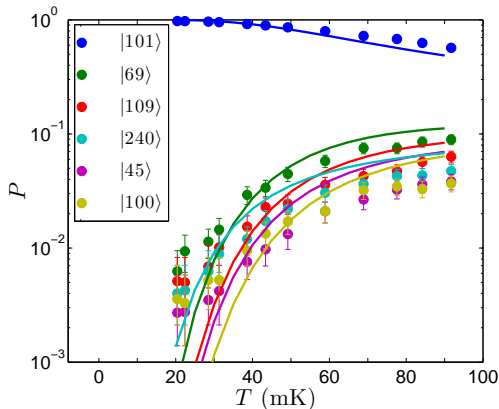
$$M_{mnkl} = -\delta_{nk}\langle l|\partial_t|m\rangle - \delta_{ml}\langle n|\partial_t|k\rangle, \quad (7b)$$

where R_{mnkl} is the so-called Redfield tensor which is constructed from matrix elements of the flux operators between eight-qubit states $|m\rangle$ and the noise spectral densities $S_j(\omega)$.

See Amin *et al.*, Phys. Rev. A. **80**, 022303 (2009) for details.

Example A Probabilities versus Temperature

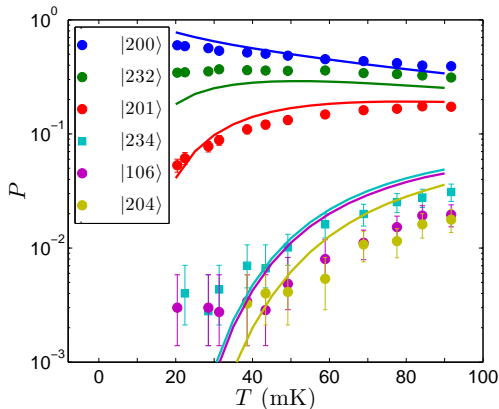
Run numerical simulation of Example A, plot probability P of observing the lowest 6 states versus T .



Data (points) and simulations (curves). Color of curves chosen to match points. Simulation had no free parameters.

Example B Probabilities versus Temperature

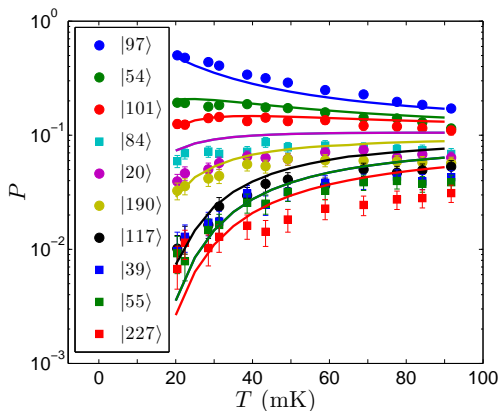
Run numerical simulation of Example B, plot probability P of observing the lowest 6 states versus T .



Data (points) and simulations (curves). Color of curves chosen to match points. Simulation had no free parameters.

Example C Probabilities versus Temperature

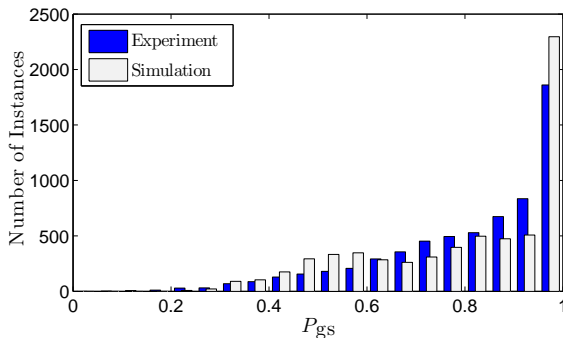
Run numerical simulation of Example C, plot probability P of observing the lowest 10 states versus T .



Data (points) and simulations (curves). Color of curves chosen to match points. Simulation had no free parameters. Note the disparity between the degenerate pairs ($|54\rangle, |101\rangle$) and ($|117\rangle, |190\rangle$).

Success Histogram at $T = 20$ mK

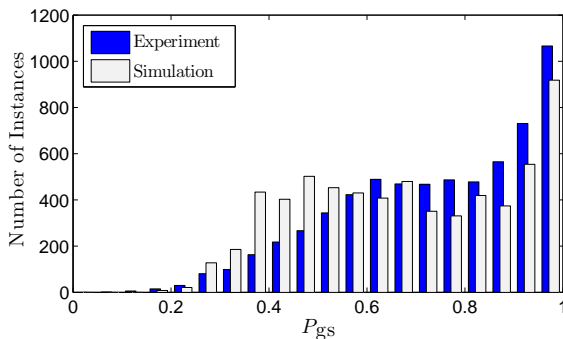
Run numerical model on all 6400 problem instances with $T = 20$ mK, generate a theoretical P_{gs} histogram.



Spike at high P_{gs} and tail to lower probability.

Success Histogram at $T = 35$ mK

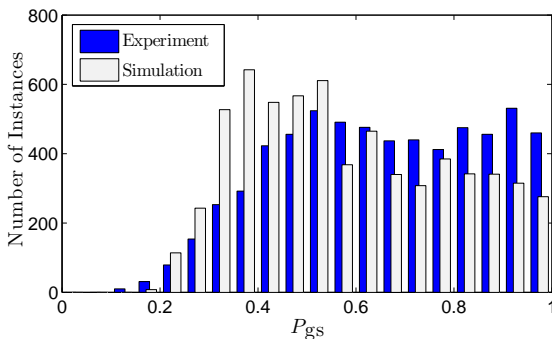
Run numerical model on all 6400 problem instances with $T = 35$ mK, generate a theoretical P_{gs} histogram.



Loss of P_{gs} from the spike and growth of broad hump near $P_{gs} \sim 0.6$.

Success Histogram at $T = 50$ mK

Run numerical model on all 6400 problem instances with $T = 50$ mK, generate a theoretical P_{gs} histogram.



Elimination of P_{gs} spike and shifting of broad hump to $P_{gs} \sim 0.5$.

Summary of Numerical Simulations

Key findings from the model:

- A quantum mechanical model of an 8-qubit system coupled to a thermal environment has been implemented.
- The model, *with no free parameters*, quantitatively reproduces the experimentally observed probabilities of the lowest lying states.
- There is some disagreement between the experimental and theoretical probabilities of observing some of the higher excited states. We are currently considering three possible causes:
 - Errors in embedding problem instances (PMM?).
 - Structure in the high frequency part of the flux noise spectral density.
 - Effects of low frequency flux noise that were not captured by the model.

Outline

- 1 Brief Recap
- 2 Qubit and Coupler Characterization
- 3 Performance of a Unit Cell
- 4 Dynamical Model of a Unit Cell
- 5 Open Questions and What Lies Ahead**
- 6 Conclusions

Outline

- 1 Brief Recap
- 2 Qubit and Coupler Characterization
- 3 Performance of a Unit Cell
- 4 Dynamical Model of a Unit Cell
- 5 Open Questions and What Lies Ahead
- 6 Conclusions**

Conclusions

- An eight-qubit unit cell of a superconducting optimization processor has been studied using a set of 6400 random Ising spin glass problems.
- The hardware always returned the ground state (the optimal solution) as the most probable state.
- The data are quantitatively consistent with a quantum mechanical model, whose parameters were independently calibrated, in which the unit cell couples to a thermal environment.

Useful References

Density Matrix Dynamical Model

Amin *et al.*, Phys. Rev. A. **80**, 022303 (2009).

Unit Cell Performance

Harris *et al.*, Phys. Rev. B **82** 024511 (2010).